Heritage Science

RESEARCH

Open Access

Analysing the glaze of a medieval ceramic fragment from the Durres Amphitheater in Albania

Maria Grazia Perna[1,2,3,4], Francesca Falcone[1,2,3,4], Chiara Casolino[1,3*], Elvana Metalla[5], Gianluigi Rosatelli[1,2,3,4], Sonia Antonelli[1,3] and Francesco Stoppa[1,2,3,4]

Abstract

The paper analyses the glaze of a ceramic sherd found in the southern sector of the Durres amphitheatre. Specifically, the sherd was found in a layer datable to the late 12th to early 13th century, which can be interpreted as a dismissal layer of a pottery kiln in use between the early and second half of the 12th century. The glaze was analysed using SEM–EDS and Total XRF techniques. The green-ocean glaze with a blue-sky decoration of the fragment has As-Co and Pb–Sn-Si compounds as pigments and phosphorous as a modifying agent and a flux. The glaze composition is SiO_2 47.6 wt.%, TiO_2 0.22 wt.%, Al_2O_3 4.08 wt.%, FeO_{total} 0.22 wt.%, MnO 0.08 wt.%, MgO 0.23 wt.%, CaO 2.51 wt.%, Na_2O 1.55 wt.%, K_2O 5.16 wt.%, P_2O_5 3.01 wt.%, SnO_2 4.13 wt.%, As_2O_5 4.13 wt.%, PbO 25.4 wt%. Fe is expressed as FeO_{total}. The trace elements composition (ppm) is Co 3684, Ni 1023, Cu 819, Zn 3070, Bi 3172, and Sr 205. We introduced a robust glaze classification scheme based on chemistry. This scheme categories the glaze as alkaline-lead SnO_2-opacified. We examined uncommon compounds formed in various textural contexts to establish the production origin and technique peculiarity. The glaze glasses form three different compositional domains: one represents the parental high-temperature initial glass composition, and two are related to immiscible segregations forming at lower temperatures. Five phases of the apatite supergroup were identified, along with other phases distributed throughout the glaze. The compounds present, such as Pb and Sn silicates, leucite, and k-feldspar and their balances, constrain the firing temperature to 720 ℃ and 900 ℃, respectively.

Keywords Alkaline-lead opacified glaze, Glaze classification, Co-as pigments, Pb-as-apatites, Durres amphitheatre (Albania), Khäsän region Iran

Introduction

The archaeological excavation between 2018 and 2022 at the southern sector of Durres amphitheatre has yielded valuable insights into the city's function during the medieval period [1, 2]. We have made remarkable discoveries by exploring the site's complex stratigraphic sequence, shedding light on how the amphitheatre influenced the integration of medieval residential architecture within its galleries. This groundbreaking research has enhanced our comprehension of the city's historical significance during the medieval era.

The amphitheatre of Durres, traditionally attributed to the Trajan period, stands with a harbour city and the Via

*Correspondence:
Chiara Casolino
chiara.casolino@unich.it
[1] DiSPuTer—Department of Psychological, Health and Territorial Sciences G. d'Annunzio University, Via Dei Vestini, 31 66100 Chieti, Italy
[2] CAST- Center for Advanced Studies and Technology G. d, Annunzio University, Via Dei Vestini, 31 66100 Chieti, Italy
[3] C.A.A.M.-Centro Di Ateneo Di Archeometria E Microanalisi G. d, Annunzio University, Via Dei Vestini, 31 66100 Chieti, Italy
[4] D.A.T.A.- U. D'A analyTicAl High-Tech Laboratory, G. d'Annunzio University, Via Dei Vestini, 31 66100 Chieti, Italy
[5] Archaeological Institute of Tirana, 1001 Tirana, Albania

Egnatia, which placed the city as a focal point connecting East and West.

The building's use as an amphitheatre can be dated to the mid-fifth century. Subsequently, the structure is reused with different functions: defensive and productive in late antiquity, funerary in the early medieval period, commercial to residential-productive, and then exclusively residential in the medieval period. Reuse for residential purposes will remain unchanged until modern times [2].

The importance of the city of Durres is closely related, therefore, to its strategic position, and this role remains unchanged even after the end of the structure's use as an amphitheatre. This role is well evidenced by the archaeological investigations conducted in the southern sector of the amphitheatre. In particular, it is worth mentioning the conspicuous amount of pottery found in the investigated stratigraphies, among which there are several imported pottery, for example, from the Italian peninsula and the Aegean area. In addition, Byzantine pottery, such as glazed pottery, sgraffito ware, and measles ware are particularly significant.

During the 2022 campaign, a significant discovery was excavating a pottery kiln [3]. This discovery provided insight into the craftsmanship of pottery production during the medieval period. Among the deconstruction layers facing the kiln, we uncovered a sherd of protostonepaste. This fragment has been identified as part of a biconical bowl from Iran, dating to the first half of the twelfth century [4]. The pottery fragment had light blue glazing and dark blue painted decorations inside. The sherd pottery is residual to of the furnace's disuse phase, while it is in phase to use the furnace (early 12th—late 12th century). Few finds of so-called stonepaste or fritware ceramics exist in the Western European area (excluding Islamic Spain). A few finds in of the Ligurian-Genovese [5] and Venetian areas [6] confirm the role of these maritime cities in relations with the East. For us, the discovery of a fragment from Raqqa Ware in Salento [7] holds excellent significance due to its pivotal cultural, technological, and commercial links with the area of *Dyrrachion* (Durres).

The pottery displays a paint applied over the glaze (Fig. 1). A comprehensive examination of the ceramic body concludes that its provenance within the Iranian region, particularly between Käshän and Qamsar [4]. The finding of this ceramic type establishes cultural ties and trade connections between Durres and the Iranian region in the medieval period. We thoroughly examined the glaze to enhance the study of the ceramic body's

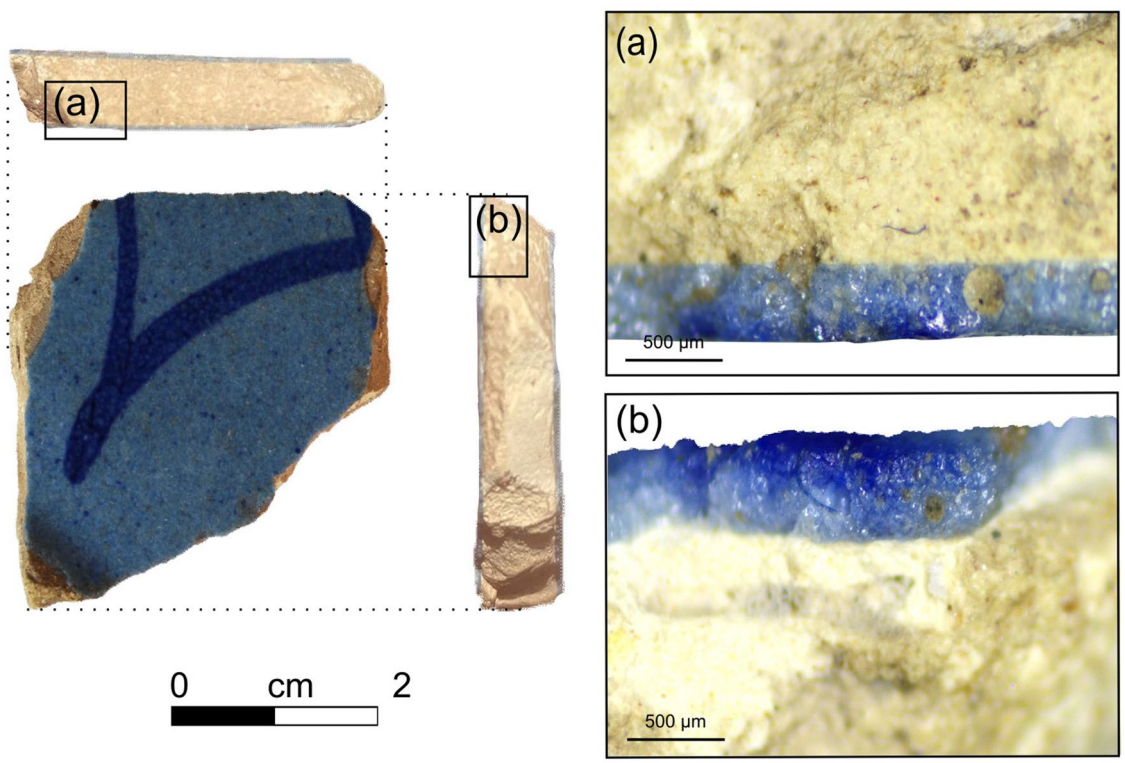

Fig. 1 Hand-scale ceramic sample from Durres. Insets (**a**) and (**b**) represent the external and internal glaze at contact with the ceramic body

consistency. This demonstrates how the study of glazes on medieval ceramics helps us to understand advances in the production of ceramic objects. Alchemical recipes could clarify why certain compounds are used in glazes, giving them a distinct appearance and making them difficult to replicate inexpensively. Alternatively, the composition of a glaze might be connected to uncommon geological sources characteristic of the region. This complex matter can only be resolved by employing comparative techniques. Our glaze contains elements like As and Co and intricate phosphate compounds. It is suggested that As was used in glazes from different regions of the ancient world, such as Egypt, Syria, Iran, and Iraq, and diffused in Islamic lands.

The primary objective of studying the glaze is to thoroughly analyse and describe it, aiding in reconstructing its origin and the techniques used in its production. By examining the glaze's attributes alongside the ceramic type, we can differentiate between locally-made items and those imported to Durres. The recognition that advanced technologies, including pottery production, spread through the historic Silk Road from the Far East to the West brings forth the difficulty of pinpointing glaze categories of akin compositions for establishing the origin and production technique of artefacts; however, the ceramic fragment's distinctive composition is rare at Durres, where was found a single fragment of fritware with origins traced back to Syria, dating to the 13th-14th century [8]. In addition, the pottery found in phase with the sherd analysed, datable to the 12th century, is glazed Byzantine pottery, the sgraffito ware, the measles ware that compares with the Aegean area, Corinth and Argos. Therefore, while not quantitatively substantial, the thorough analysis of this sherd holds considerable qualitative significance, emphasising its potential role in delineating trade routes and cultural interactions.

Methods

The glaze was analysed at D.A.T.A.-U.D'A analyTicAl High-Tech Laboratory in the G. d'Annunzio University in Chieti, Italy. OPTECH and Zeiss optical microscopy were used to study the glaze in thin sections. The chemical composition of the glaze was detected by scanning electron microscopy Phenom XL SEM–EDX. Most accurately, the backscattered electrons microscope imaging mode was used in BSE images, in which the different phases present could be distinguished based on their atomic number contrast. The total reflection X-ray fluorescence analysis to detect the trace elements of glaze composition was performed by TXRF Horizon (GNR), with Mo–Ka excitation energy, working at 40 kV and 15 mA. SEM–EDX and TXRF microanalysis has been applied here as a new methodological approach for characterising glaze materials. The data acquired through the two analytical techniques has been processed with a mathematical calculation to obtain an accurate ratio of elements and precise data from the samples. The micro-analytical method was also carried out on soil standards JG-3, GBW-07045, GBW-07405, and NIST to validate the analytical data on our sample [9].

Results

Petrography

The glaze is semi-opaque and has a pearly, glassy sheen with a brilliant refraction effect. Under a reflected light microscope, the surface of the glaze appears slightly wavy with lighter and darker areas. There are no visible bubbles or cracks on the surface. The glaze displays an ocean-green background with RGB values of 85, 128, and 105 and a Pantone colour code of 625 C. The decoration is a blue sky with RGB values of 0, 210, and 194 and a Pantone colour code of 3265 C (Fig. 1). The design seems to have been created using the blue-sky glaze fired on top of the ocean-green glaze (Fig. 1).

The thickness of the glaze is about 500 μm. Under Scanning Electron Microscope (SEM), a dense network of crystals can be seen branching out on the surface of the glaze. We found silica crystals and skeletal euhedral and hexagonal crystals of As-Pb apatites (Figs. 2 and 3). The silica crystals consist of a felt-like arrangement of prismatic crystals up to 100 μm long but only 1–2 μm thick. They can be subdivided into dendritic or radiate aggregates. This type of structure is typical of melts that have been quenched.

The glaze is opaque due to scattered aggregates of 1–2 μm crystals of Sn oxides, which form sparsely distributed patches. The polished section of the glaze shows relics of quartz and K-feldspar. Larger rounded quartz fragments show overgrowth of euhedral prismatic silica crystallites and sometimes lead silicate. Clusters of euhedral crystals of neo-formed K-feldspar are present, along with strongly leucite. Euhedral prisms of silica crystallised in plastic segregation are common. These plastic segregations have a well-defined contour and differ from the surrounding glass. Apatite minerals are widely distributed in the glaze. Large, scattered vesicles up to 80 μm are typical. These vesicles are either empty or internally filled with phosphates and lead silicate crystallites.

Glass and minerals composition in glaze

The archaeometric study involves the definition of mineral phases with stoichiometry derived from the mineral's crystal structure, which is relatively fixed.

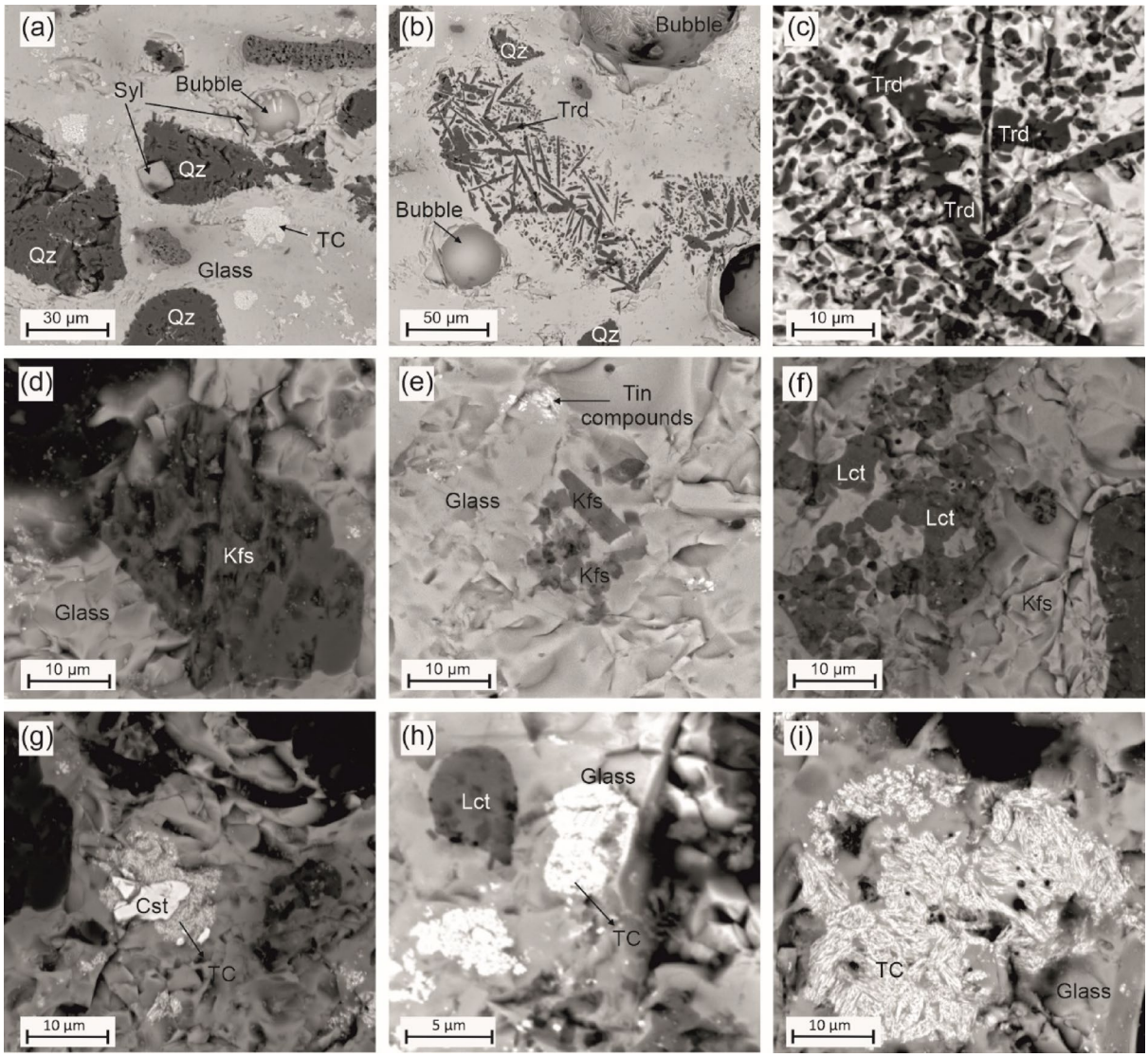

Fig. 2 SEM-EDAX BSE greyscale image of the composition and morphology of the glaze. **a** Residual quartz with tridymite overgrowth, sylvite euhedral, and aggregates of tin compounds in the glass matrix; **b** Spinifex texture of tridymite in ameboid immiscible glass segregation; **c** Incipient symplectic structure formed by tridymite and K-feldspar; **d** Residual orthoclase plus quartz microliths; **e** Neo-formed laths of sanidine in the glass; **f** Corroded leucite in reaction with sanidine; **g** Residual pure Sn oxide, cerussite; in reaction with the surrounding glass forming tin–lead silica compounds; **h** and **i** Details of aggregates of tin compounds in glass. *Qz* quartz, *Syl* sylvite, *Trd* tridymite, *Kfs* K-feldspar, *Lct* leucite, *Cst* cassiterite, *TC* tin compounds

Glass

Outer glaze glass composition Chemical compositions of blue-sky and green-ocean glasses, obtained by SEM analyses, are in Table 1.

Substantial differences exist in the As_2O_3/CoO ratio (Fig. 4a). The blue-sky decoration has a moderate As_2O_3/CoO ratio of around 1.8. In contrast, the green-ocean glass has a remarkably high As_2O_3/CoO ratio of about 60. The As_2O_3 and CoO proportion of 2:1 resembles that of cobaltite (CoAsS) oxide composition (i.e., CoO at 28.6 wt.%, As_2O_3 at 44.7 wt.%, and S at 19.3 wt.%) [10]. Notably, As/Co ratios depend on the ore's ores and roasting process [11, 12].

In the triangular diagram of SiO_2 vs. PbO vs. all other elements, the glasses overlap in a restricted field with a low-lead alkaline composition (Fig. 4b) (after [13, 14]).

Inner glaze composition Glaze-body glass composition notably differs from the surface and shows a greater variability. The average composition is SiO_2 45.9 wt.%, Al_2O_3 2.75 wt.%, CaO 1.6 wt.% Na_2O 0.89 wt.%, K_2O 4.3 wt.%, PbO 43.9 wt.%, As_2O_3 0.66 wt.%. In the conventional

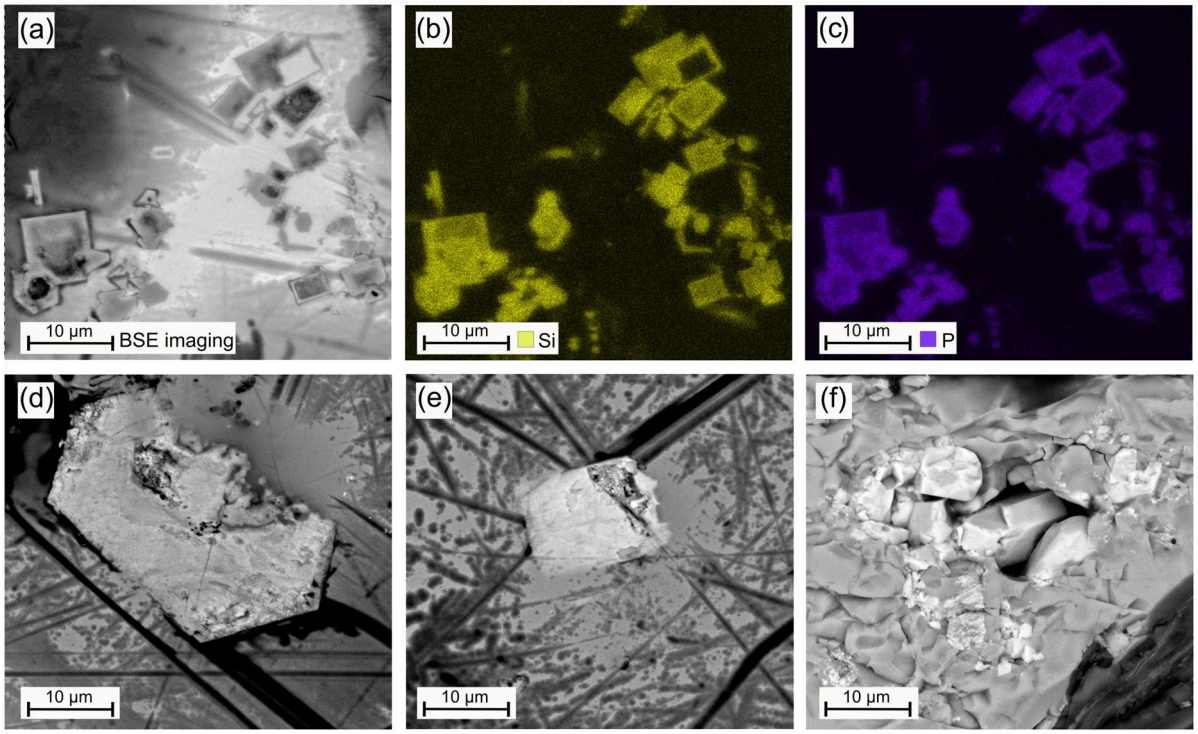

Fig. 3 SEM-EDAX BSE grey scale image of the different apatite types in the glaze. **a** BSE imaging of skeletal zoned apatite type 1 crystal; Same as (**a**) elements distribution in false colours highlighting Ca (yellow) (**b**) and P (purple) (**c**); (**d**), (**e**) apatite type 2; (**f**) apatite type 3

Table 1 chemical compositions of blue-sky and green-ocean glasses, obtained by SEM analysis

Oxides (wt.%)	Blue-sky glasses	Green-ocean glasses
SiO_2	52.0	54.6
Al_2O_3	4.70	4.20
FeO_t	1.50	0.60
MgO	1.20	0.80
CaO	1.30	1.40
Na_2O	3.00	3.60
K_2O	6.20	5.30
P_2O_5	2.70	2.70
PbO	24.1	25.0
As_2O_3	0.90	0.70
CoO	0.50	bdl

SiO_2-PbO-$Na_2O+K_2O+Al_2O_3+As_2O_3+CaO$ diagram (Fig. 4c), the glasses follow a definite trend with moderate PbO content (43.9 wt.%) and low alkali content (5.2 wt.%).

Two groups of glass compositions can be distinguished by their different elemental contents. One group is characterised by low PbO and high Na_2O+K_2O, related to the crystallisation of feldspars and leucite. The second group has higher PbO and lower Na_2O+K_2O, which is related to the crystallisation of silica (tridymite). These latter glasses have a higher PbO/SiO_2 ratio (>1) (Fig. 4d) and a very constant ratio of other elements between 6.5 and 8.5 wt.% of $CaO+Na_2O+K_2O+Al_2O_3+As_2O_3$ (Fig. 4c). On the other hand, after the crystallisation of leucite plus K-feldspar, the glass has a high $CaO+Na_2O+K_2O+Al_2O_3+As_2O_3$ above 10 wt.% (Fig. 4c) and a low PbO/SiO_2 ratio below 0.8 (Fig. 4d).

Silica

Silica can form several different structures depending on temperature variations and glass composition. Large, irregularly shaped quartz crystals show overgrowth of small tridymite laths (Fig. 2a). Additionally, tridymite forms a spinifex texture only in discrete areas of glass segregations that are chemically different from the rest of the glass (Fig. 2b and c). The plastic shape of these areas suggests immiscibility between glasses with varying concentrations of Si, Pb, P, and As. Silicate liquids at relatively low temperatures exhibit immiscibility gaps between the saturated SiO_2 component and the undersaturated SiO_2 component. In nature, this phenomenon is widely observed between mafic (basaltic) and felsic

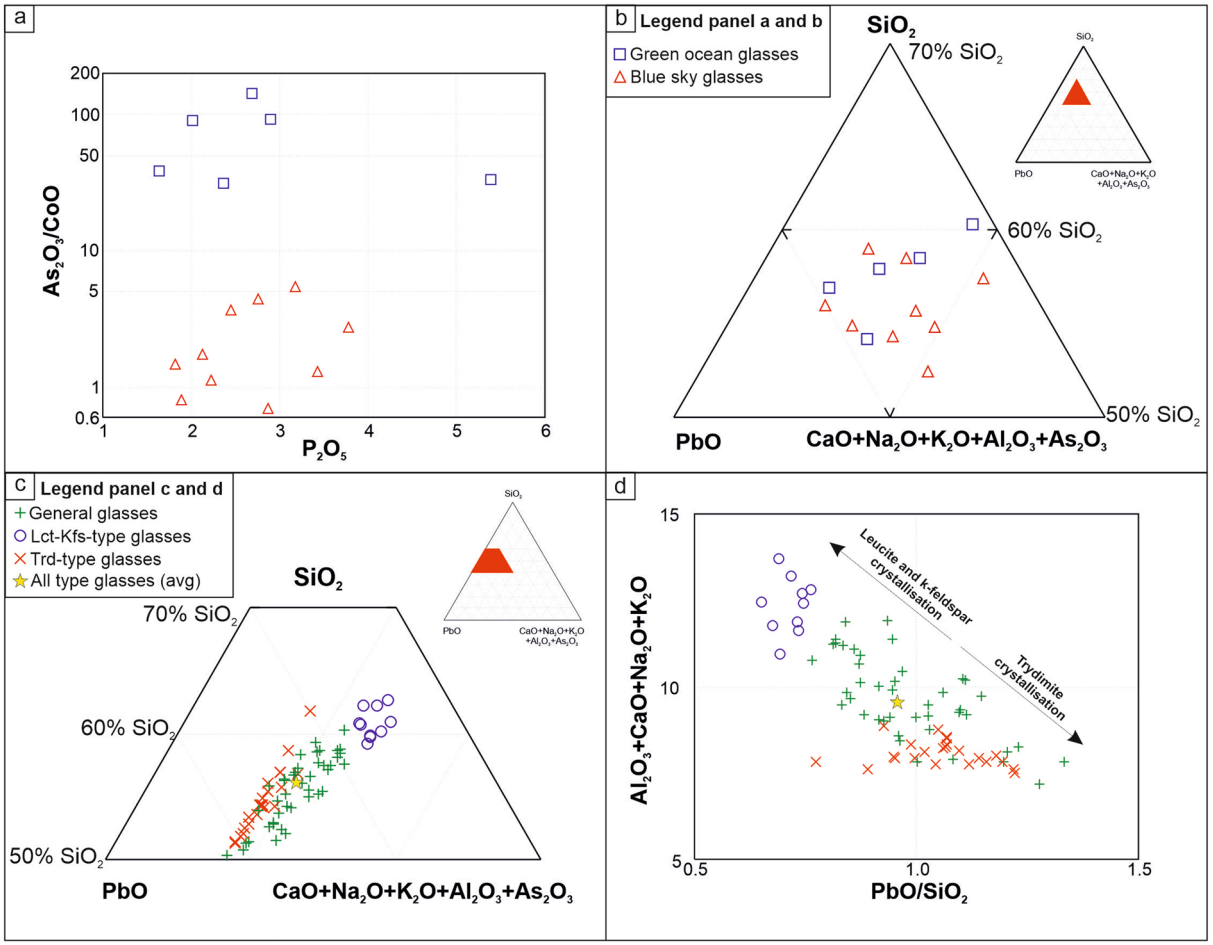

Fig. 4 Classification diagrams for glasses from the surface and the body of the glaze. **a** Bivariate diagram As_2O_3/CoO vs P_2O_5 (in wt.%) for the glasses in the blue-sky decoration and the green-ocean matrix. **b** SiO_2-PbO-Al_2O_3 + CaO + Na_2O + K_2O + As_2O_3 (in wt.%) classification diagram for the glass in the blue-sky decoration and the green-ocean matrix (modified following [13]). Grading ranges from 70 wt.% SiO_2 to 50 wt.% SiO_2. **c** SiO_2-PbO-Al_2O_3 + CaO + Na_2O + K_2O + As_2O_3 (in wt.%) diagram for glass in the glazed body (modified following [13]). Grading ranges from 70 wt.% SiO_2 to 50wt.% SiO_2. **d** Bivariate diagram Al_2O_3 + CaO + Na_2O + K_2O (in wt.%) versus PbO/SiO_2 ratio shows the glasses' crystallisation trend correlated with the different mineralogical phases. All type glasses (avg) refer to the average composition of all the glasses (Lct-Kfs-type glasses; Trd glasses; General glasses). Glass composition analyses are in Additional file 1: Table S2

(granitic) liquids [15]. This process is also likely to occur in artificial silicate liquids.

Furthermore, the texture suggests possible incipient eutectic crystallisation of K-feldspar + tridymite. Immiscibility features are also apparent in Fig. 4, where the glass associated with tridymite contains significant amounts of K, Al, and Si, capable of crystallising K-feldspar. Although we did not find a close textural relationship between K-feldspar and tridymite, incipient intergrowth structures are apparent from the micrographic texture adopted by the semi-oriented tridymite crystals (Fig. 2c).

K-feldspar—Leucite

The feldspars occur in two different paragenetic and textural associations. Orthoclase with an average stoichiometric formula of $(K_{0.87}Na_{0.10})_{0.97}Al_{1.00}Si_{3.03}O_8$ was added as a flux and partially reacted with the lead silicate melt. It also occurs in small lithics composed of quartz and orthoclase of granitic origin (Fig. 2b and d). This lithotype is the source from which the mixture used to form the silica-alkaline components of the glaze recipe was obtained.

The orthoclase differs from small aggregates of euhedral newly formed K-feldspar (sanidine) (10 µm) disseminated in the glaze (Fig. 2d). The freshly formed K-feldspar is very pure, with no Na present, and has an average composition of $K_{0.88}Al_{1.00}Si_{3.23}O_8$.

K-feldspars also occur associated with newly formed leucite. Leucite forms large patches of composite anhedral or subhedral crystals with clear engulfment due to

resorption and disequilibrium with the surrounding glass (Fig. 2e and f). The average composition of leucite is $K_{0.96}Al_{1.00}(Si_{1.77}Al_{0.26})_{1.93}O_6$.

Tin compounds

Tin is a crucial component in the opaque lead glaze. Divalent and tetravalent Sn compounds form a complex reaction pattern when reacting with the lead glass, modifying the glaze's physical properties. For example, Sn^{4+} has low solubility, but Sn^{2+} divalent forms metastable phases in phosphate and arsenate lead silicate glasses [16]. Sn^{2+} ions dissolved in glassy network whereas Sn^{4+} ions precipitate as cassiterite when amount is higher than 6–8 wt% (e.g. [17]).

Discrete anhedral crystals of almost pure Sn oxide are present and are characterised by a striking reaction with glass to form microcrystals of variable compositions (Fig. 2g). With further progression of the reaction of SnO_2 with the melt, a broad patch of crystallites is formed, associated with the disappearance of each pure SnO_2 crystal and the formation of compact aggregates of Sn and Pb silicates (Fig. 2h and i), with an average composition of $(Sn_{0.71}Pb_{0.22})_{0.93}(Si_{0.95}\ Al_{0.10})_{1.05}O_3$. The analytical reproducibility and euhedral contour suggest a mineral not yet accepted by the IMA (International Mineralogical Association) and requires further investigation.

Apatite supergroup

An essential feature of this structural group is its ability to incorporate a range of vicariant elements on the Ca and P sites. The general formula of the group, consisting of more than 20 mineral species, can be expressed as $^{IX}M1_2{}^{VII}M2_3(^{IV}TO_4)_3X$ with M = Ca^{2+}, Pb^{2+}, Ba^{2+}, Sr^{2+}, Mn^{2+}, Na^{+}, Ce^{3+}, La^{3+}, Y^{3+}, Bi^{3+}; T = P^{5+}, As^{5+}, V^{5+}, Si^{4+}, S^{6+}, B^{3+}; X = F, (OH), Cl [18]. Notably, the apatite minerals of the pyromorphite–mimetite series, $Pb_5(PO_4)_3Cl$–$Pb_5(AsO_4)_3Cl$, are rare and crucial for their physical properties [19, 20]. In the glaze, phosphates were crystallised in five occurrences corresponding to different molar solutions: apatite, pyromorphite, britholite, mimetite, and johnbaumite. The main chemical features are shown in Additional file 1: Figure S1, and representative analyses are provided in Additional file 1: Table S1. In Figure S1a, a mixture of hedyphane, apatite, and pyromorphite trends evolve in a continuous series up to an extreme term of mimetite and johnbaumite. Furthermore, when we examine the molar mixtures of these end-members, it becomes possible to distinguish several molar mixtures that are distinct from each other. Most of these align with britholites and apatites, while the remainder correspond to a combination of johnbaumite and mimetite (Figure S1b).

The first 20 µm of the blue-sky glaze surface contains oscillatory zoned, skeletal hexagonal euhedral apatite (type 1), 5 µm in diameter, clustering as an intergranular phase among tiny silica prisms (Fig. 3 a, b and c). They are a mixture of end-members of the apatite group containing As and Pb. The average molar solution has a composition of $(Ca_{2.63}Pb_{0.17}Na_{2.03}\ As^{3+}{}_{0.11})_{4.94}\ (P_{2.09}Si_{0.88}\ As^{5+}{}_{0.07}O_4)_{3.04}$, a molar solution composed of 62% hydroxyl-apatite, 28% britholite, 8% mimetite, 6% johnbaumite and 4% pyromorphite. The oscillatory zonation results from a variation of P + Ca versus Si.

Larger unzoned microcrystals and crystallite aggregates are also sparsely present in the ocean-green glaze. In this portion, euhedral crystals are found whose formula is $(Ca_{2.82}\ Pb_{0.89}Na_{1.22})_{4.93}(P_{2.03}Si_{1.03}O_4)_{3.06}(Cl_{0.25})$. The molar solution is dominated by 51% apatite, 33% britholite, and 16% pyromorphite, while terms with As (johnbaumite and mimetite) are characteristically absent.

Apatites are mostly aggregates of subhedral to anhedral-zoned microcrystals (apatite type 2) (Fig. 3d and e) and are highly heterogeneous regarding molar composition. Apatite type 2 zoning ranges from the core to the rim with a proportional increase in mimetite and johnbaumite end-members:

1. core: $(Ca_{2.65}Pb_{1.86}Na_{0.6}As^{3+}{}_{0.39})_5(P_{1.32}Si_{0.79}As^{5+}{}_{0.89}O_4)_3(Cl_{0.27}F_{0.13})$ and molar composition hydroxyl-apatite 23%, brytholite 23%, johnbaumite 22%, mimetite and pyromorphite 16%, respectively.
2. intermediate: $(Ca_{2.20}Pb_{2.34}Na_{0.08}As^{3+}{}_{0.38})_5(P_{0.95}Si_{0.70}\ As^{5+}{}_{1.35}O_4)_3(Cl_{0.26}F_{0.04})$ and molar composition mimetite 27%, johnbaumite 25%, britholite 21%, apatite and pyromorphite 14%, respectively.
3. rim: $(Ca_{1.83}Pb_{2.64}As^{3+}{}_{0.43})_{4.90}(P_{0.10}Si_{0.67}As^{5+}{}_{2.23}O_4)_3(Cl_{0.33})$ and molar composition mimetite 46%, johnbaumite 32%, britholite 19%, pyromorphite 2% and apatite 1%, respectively.

Apatite type 3 occurs as euhedral larger crystals in miaroles or as internal wrapping or filling of vesicles (Fig. 3f). Their composition matches the formula $(Ca_{1.97}Pb_{2.48}\ As^{3+}{}_{0.54})_{4.99}\ (As^{5+}O_4)_3$ and molar composition mimetite 56% and johnbaumite 44%, similar to lead-calcium other arsenate compounds [21, 22].

Finally, apatite type 4 occurs as subhedral crystallites up to 3 µm in abundant discrete crystallites in isolated patches in the glass of the glaze. The average stoichiometric formula is $Ca_{3.09}Pb_{1.93}\ (As^{5+}{}_{2.44}Si_{0.53}O_4)_{2.97}O_3(Cl_{0.45})_{1.00}$, which is consequently classified as hydroxyl-headphone.

Glaze chemistry

The average composition of the glaze is in Table 2. Other chemical characteristics are a PbO/SiO_2 ratio of 0.53, an

Table 2 Average composition of the glaze

Oxide	Wt%	Oxide	Wt%
SiO_2	47.6	SnO_2	4.13
TiO_2	0.22	As_2O_5	4.13
Al_2O_3	4.08	PbO	25.44
FeO_t	0.22	**Element**	ppm
MnO	0.08	Co	3684
MgO	0.23	Ni	1023
CaO	2.51	Cu	819
Na_2O	1.55	Zn	3070
K_2O	5.16	Bi	3172
P_2O_5	3.01	Sr	205

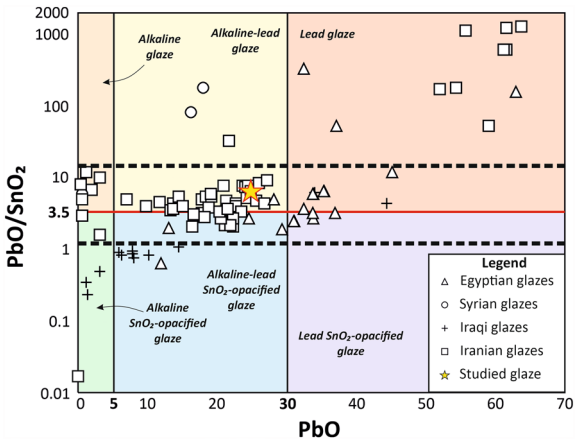

Fig. 5 Classification scheme for glazes. The scheme is based on the ratio of alkali content to lead content (as [24]), dividing the three fields of alkaline glaze, alkaline-lead glaze and lead glaze, and on the ratio PbO/SnO_2. with divisor at 3.5, (following [23]), that represent a weighted average in the field of typically opacified glazes. The data used are from [26–29]. The dotted lines correspond to PbO/SnO_2 from 20 to 2 for Ottoman, Timurids, and associated productions and between 3 and 6 for Iznik productions [30]

Alkalinity Index (A.I. = $(Na_2O + K_2O)/Al_2O_3$) of 1.65 and Na_2O-2 < K_2O, giving a potassic character to the glaze.

We propose a classification scheme based on a PbO/SnO_2 ratio equal to 3.5, dividing SnO_2-opacified glaze from others following the flow chart of [23] and on the conventional classification in alkaline, alkaline-lead, and lead glaze based on the ratio between alkali and lead [24]. The new classification scheme is based on robust chemical data. Furthermore, additional information classifying the glazes based on geographic origin allows us to compare the sample in the study with alkaline-lead SnO_2-opacified Iranian glazes [25].

The glaze studied is an alkaline-lead SnO_2-opacified glaze (Fig. 5).

In the conventional triangular diagram of [6], our sample was plotted together with a dataset of 172 samples from Iran, Iraq, Egypt, and Syria (Additional file 1: Figure S2). From a geographical point of view, our glaze falls close to the cluster of Iranian glazes (Additional file 1: Figure S2a). However, some Egyptian and Syrian glazes samples were also plot near our sample (Additional file 1: Figure S2a).

From the point of view of SnO_2 content, in the diagram of [6], glazes with a PbO/SnO_2 ratio greater than 3.5 confirm classification as alkaline-lead SnO_2-opacified (Additional file 1: Figure S2b). Our glaze can be compared with lustre, opaque, blue, and turquoise glazes (Additional file 1: Figure S2c-f). The glaze is close to the blue and turquoise Iranian plotting field.

Body composition

The ceramic specimen discovered in the Durres amphitheatre's southern sector shares similarities with earthenware and protostonepaste. However, it exhibits a more pronounced association with protostonepaste, particularly in normative mineralogical composition, specifically the alkali feldspars, quartz, and clay minerals ratio. It is characterised by a meticulously balanced amalgamation of crushed kaolinised leucogranite, frits, and talc. Our investigation suggests that the ceramic traces its origins to Iran, specifically the Käshän and Qamsar regions, dating back to the 12th century. The ceramic body is the subject of a dedicated paper [4].

Discussion

The main characteristic of the glaze studied is the presence of two different immiscible domains (glass + minerals), one characterised by the crystallisation of tridymite and the other by the crystallisation of alkaline minerals (leucite and k-feldspar). Notably, immiscibility occurs only in the innermost part of the glaze and is proximal to the ceramic body. We interpret and discuss this observation by assuming that the immiscibility phenomenon is due to a greater temperature drop than that of the surface, whose homogeneous composition was quenched at the end of the firing process. These characteristics seem to us to be more peculiar than the general mineralogical composition. However, there are some parallels in the literature, e.g. the presence of phosphates and Sn and Pb compounds.

First, by comparing the silicon dioxide (SiO_2), aluminium oxide (Al_2O_3), and alkali content of the glaze and removing all other elemental components, we deduce that the glaze was produced by adding 20% potassium feldspar and 58% quartz—K-feldspar yields potassium to the melt. Potassium reacts with the melt, forming

new phases, such as sanidine and leucite, during cooling (Fig. 5a).

Pb and Sn silicates, due to the high solubility of PbO in glass, decompose to form SnO_2, resulting in aggregates of PbO-SnO_2-SiO_2 microlites in irregular patches embedded in the lead glass. These Pb and Sn silicate compounds crystallise phases that resemble the compound known in the literature as lead–tin yellow I (Pb_2SnO_4) and lead–tin yellow II ($PbSn_2SiO_7$). These are compounds that, in our case, have crystallised in the form of a mineral with its stoichiometry $(Sn_{0.71}\ Pb_{0.22})_{0.93}\ (Si_{0.95}\ Al_{0.10})_{1.05}\ O_3$, as described in the previous paragraph 3.5. Lead–tin yellow II, whose probable composition is identified by [31], was synthesised between 800℃ and 950 ℃ by [32] from a mixture of lead–tin yellow I and silica [33]. The chemical composition we refer to as these compounds is the product of an initial interaction of lead–tin yellow I with silica, which led to the formation of lead–tin yellow II, SnO_2 and SiO_2. Recombination of these compounds resulted in the mixture we found. [32] also considers lead–tin yellow as a glass opacifier.

A significant difference exists between state diagrams involving peritectic and eutectic leucite-k-feldspar and tridymite and state diagrams using compounds without considering their crystal structure. The latter is mainly used in ceramics. It is not easy to draw a parallel between the two. If we omit to consider the temperature data provided by mineralogical state diagrams and use only those for the compounds in ceramic glazes, we obtain results that fit better with the known firing temperatures of the ceramic materials themselves.

The range of temperatures at which these transformations occur depends on the composition of the mixture; the higher the PbO/SiO_2 ratio, the more stable the particles [24]. The diagram in Fig. 5b, taken from [34] and [35], shows us that starting from the composition of our glaze (Melt) during cooling, we intersect eutectic point (PbO^*SiO_2 + quartz) at a temperature of 760 ℃, with a ratio of PbO/SiO_2 equals to 0.53, that matches well with the eutectic point. These temperatures agree with known data in the SiO_2-Al_2O_3-K_2O system in which the various eutectics give temperature estimates for both the tridymite—quartz phase (temperature 720 ℃) and the leucite—k-feldspar eutectic with a minimum temperature of 810 ℃ and a maximum temperature of 1140 ℃. The latter is not reasonable in the case of our glaze as it corresponds to mullite crystallisation, which is not present in our case. Consequently, considering the combination of the diagrams described above, our glaze's final firing temperature range is between 720 ℃ and 900 ℃ (Fig. 6).

Arsenic is a flux that lowers the melting point of the glaze and a pigment. In our case, phosphorus reacts with arsenic trioxide (As_2O_3) to form an unusual

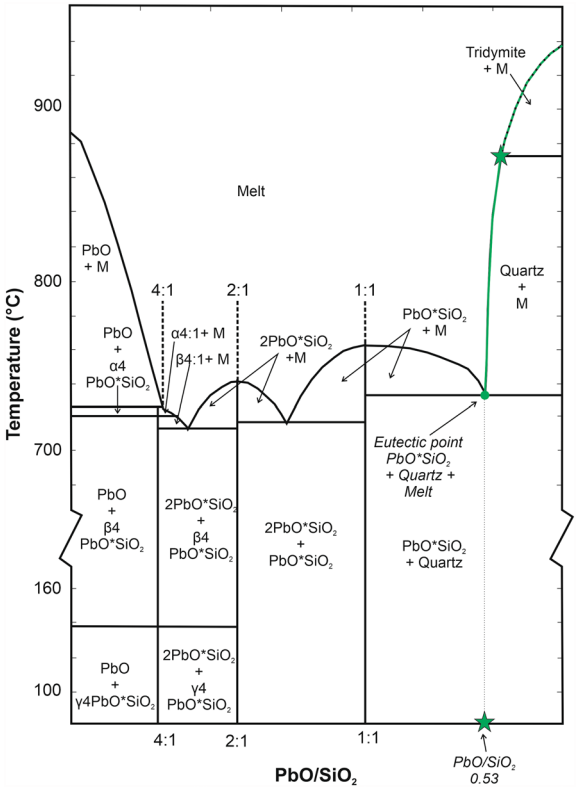

Fig. 6 PbO/SiO_2 ratio diagram, modified from [34] and [35]. The green star represents our composition and the green line represents the crystallisation path

sequence of apatite crystallisation. Also, the presence of mimetite s.s., lead chloroarsenate, is known in the literature mainly as an alteration product (which could be our case, as the OH mimetite we found crystallises in the bubbles). The sequence of minerals in the apatite supergroup shows gaps among the various mixtures, indicating crystallisation at different times. The end-member solubility is linked to different temperatures, volatile fugacity, and redox conditions. These compositions also correspond to different textural situations. For example, the mixture of britholite and hydroxyl-apatite is more common in rapidly cooled surfaces. At the same time, terms with arsenic seem to be relegated to late crystallisation forms such as miaroles and vesicles. The crystallisation of apatites leads to an undersaturation of phosphorus in the glass at the end of the process. It thus prevents further crystallisation of phosphates, favouring the crystallisation of arsenic-lead compounds. From a compositional standpoint, our glaze aligns with the typical compositions of medieval alkaline-lead SnO_2-opacified glazes (e.g., [18]). Peculiar features of the glaze are the presence of As and Co, used as blue and green pigments (e.g.,

[11]). Different decoration colours correspond to different As/Co ratios of glass compositions.

For example, blue-coloured glasses show a lower As/Co ratio, suggesting the addition of cobaltite and CoO. It is known from the literature that the addition of only 0.05 wt.% of Co is sufficient to obtain bulk glass blue, and only 0.5 to 1 wt.% of cobalt is needed for a darker blue hue [11]. Green-coloured glass has a higher As/Co ratio, suggesting that Co derives from cobaltite. Blue glazes produced using Co are typical of Iran, where Co ores are widespread close to Käshän (e.g., secondary deposits at Talmessi and Meskani and the cobalt mine of Qamsar) [36, 37]. Asserted that Persian cobalt ores are in the arsenical form and Chinese cobalt ores are, without exception, in the form of asbolite. Because of spectrographic analytical data published by [36, 37], Khamsar, near Käshän, was suggested to be the most likely source of supply for cobalt since it contained arsenic. Around AD 1425, a significant shift in the chemical makeup of the blue pigment occurred, transitioning from an arsenic-containing cobalt ore to one abundant in manganese (asbolite) [11, 38]. Other worldwide Co deposits have significant amounts of Ni, Zn, Bi, and Ag not found in the studied glaze. The production site is Iranian, characterised by the absence of Co ore association with other elements. Iranian art and culture thrived during the twelfth and thirteenth centuries, leading to the advancement of mining techniques and activities. For example, the blue enamel of the "Saljuqi" tile was obtained from the cobalt mine at Qamsar (Käshän) and widely exported with potteries in the Islamic world [39].

We also detected other modifying agents, such as copper (Cu) and relatively small amounts of bismuth (Bi), manganese (Mn), and iron (Fe).

Regarding the chemical and mineralogical evolution of the glaze, we observed a complex immiscibility phenomenon that leads to various compositional domains of both the melt and the mineral phases that crystallise from it. This phenomenon is visible in the segregation structure in the glaze, which can range in size from tens to hundreds of microns. In both textural and compositional terms, we found segregation of plastic form capable of crystallising silicon dioxide (tridymite) or an association of alkaline minerals with different silica saturation, such as K-feldspar and leucite. These variations are also reflected in the chemistry of the glasses. The ratio of PbO/SiO_2 remains constant, while the Agpaitic Index (AI) depends on the crystallising phases. In the case of tridymite crystallisation, the AI reaches a maximum value of 2.4. In contrast, if the feldspar and feldspathoid phases crystallise, the AI drops to 1.4.

Conclusions

1. The miscible phase of the glaze contains tridymite on liquid, indicating a high temperature at the surface and its stabilisation by quenching of the surface itself. The inner part, in contact with the ceramic body, apparently underwent a different thermal pathway, leading to immiscibility and separation of two immiscible compositional domains, one with tridymite and one with leucite and k-feldspar.
2. Adding P and As produced a complex phosphate arsenate sequence, indicating a progressive P recombination with As, Ca and Pb during the firing process. Texturally, it is evident that these compounds hold distinct positions concerning the other mineral phases present. Phosphate ligands can cause brittleness in glaze if they remain during melting.
3. In parallel with the crystallisation sequence of arsenate phosphates, we have the development of minerals with reproducible stoichiometry composed of Sn–Pb-Si. In particular, these mineral compositions approximate those of the non-natural, non-crystalline compounds used as pigments, commonly referred to as lead–tin yellow I and lead–tin yellow II. By this, we mean that such minerals have not yet been found in nature and are a peculiarity of ceramic glazes.
4. We propose a new classification scheme for glazes based on a PbO/SnO_2 ratio of 3.5 and PbO. Chemical datasets include information about the geographic origin of the glazes. It aligns with the typical compositions of Iranian alkaline-lead SnO_2-opacified glazes. As and Co are pigments, and P is a glaze modifier. Different decoration colours correspond to different As/Co ratios in glass compositions.
5. Trydimite on the liquidus curve indicates a minimum temperature of 900 ℃. On the other hand, the presence of leucite also indicates a high temperature. Combining the ceramic diagrams of the PbO/SiO_2 type with those known for the leucite-K feldspar-silica system, we obtain a minimum T of 720 ℃ for the different eutectics present.
6. The sherd is an underglaze painted with a knot back decoration widespread in the Iranian area. This decorative motif can be dated chronologically to the mid-second half of the 12th century. The context of its discovery confirms this dating.

Supplementary Information

The online version contains supplementary material available at https://doi.org/10.1186/s40494-024-01175-8.

Additional file 1: Figure S1. a Evolution of apatite supergroup composition in terms of (P+Si)/(Ca+Pb) vs As/(Ca+Pb). **b** Molar solution of the different groups of the apatite supergroup minerals. Apatite supergroup composition analyses are in Additional file 1: Table S1. **Table S1.** Chemical composition of apatite group minerals. **Table S2.** Chemical compositions of the different type of glasses. **Figure S2.** Conventional SiO_2-PbO-Al_2O_3+CaO+Na_2O+K_2O+FeO+MgO (in wt.%) classification diagram for the glaze (following [6]). Grading ranges from 80 wt.% SiO_2 to 30 wt.% SiO_2. The data used are from [15–18].

Acknowledgements
The fieldwork for this study was supported and co-funding by the Archaeological Institute of Tirana (Albania), the University of Chieti (Italy), and the Italian Ministry of Foreign Affairs-MAECI and supported by the Ministry of Culture (Albania). The funding organisations did not influence the study design, data collection and analysis, publication decision, or manuscript preparation. We would like to thank Dr Serenella Mancini for her valuable suggestions.

Author contributions
Conceptualisation MGP, FF, CC, SA, FS; method MGP, FF; validation GR, investigation MGP, FF, CC, SA, FS; funding FS, SA; instrumental resources GR, FS; data curation MGP, FF; original draft preparation MGP, FF, CC, SA, FS; writing review GR; editing MGP, FF, CC, EM, GR, SA, FS; figures curation MGP, FF; supervision GR, FS, SA. All authors read and approved the final manuscript.

Funding
The University of Chieti-Pescara provides open-access funding. The Italian Ministry of Foreign Affairs-MAECI, the University of Chieti (Italy) and the Archaeological Institute of Tirana (Albania) supported and co-funded this study's fieldwork.

Availability of data and materials
All data generated or analysed during this study are included in this article, and no datasets were generated or analysed during the current study.

Declarations

Ethics approval and consent to participate
Not applicable.

Competing interests
The authors declare no competing interests.

Received: 28 October 2023 Accepted: 9 February 2024
Published online: 08 March 2024

References

1. Antonelli S, Metalla E, Casolino C, Moderato M, Pallotta I. Rezultatet e gërmimeve arkeologjike në Amfiteater, vitet 2018–2019 (Results of the archaeological excavation in the Amphitheatre of Durres (2018–2019) . Candavia. 2020;20:359–77.
2. Antonelli S, Casolino C,Metalla E. Trasformazioni nell'anfiteatro di Durres in età medievale: spazi abitativi e produttivi (Transformations in the amphitheatre of Durres in the Middle Ages: living and productive spaces). Temporis Signa XVIII (in press, 2023)
3. Antonelli S, Metalla E, Casolino C. Rezultatet e gërmimeve arkeologjike në Amfiteater, vitet 2021–2022 (Results of the archaeological excavation in the Amphitheatre of Durres (2021–2022). Candavia 10 (in press, 2023)
4. Casolino C, Falcone F, Perna MG, Metalla E, Rosatelli G, Stoppa F, Antonelli S (unpublished results). Exploring Durres between East and West: discovery of a protostonepaste. Archaeological context and archaeometric analysis.
5. Benente F. Imported ceramics from the Mediterranean between the 10th and 14th centuries Updates and summary data for Liguria. In: Gelichi S, Baldassarri M, editors. Pensare/Classificare. Studi e ricerche sulla ceramica medievale per Graziella Berti. Firenze: All'Insegna del Giglio; 2010. p. 53–70.
6. Gelichi S, Negrelli C, Ferri M, Cadamuro S, Cianciosi A, Grandi E. Importing, producing and consuming in the Venetian lagoon from the 4th to the 12th century. Amphorae, glass and ceramics. In: Gelichi S, Negrelli C (eds). Adriatico Alto Medievale (VI- XI secolo). Venezia: Scambi, porti, produzioni, Edizioni Ca' Foscari. 2017. p. 23–113.
7. Caprino P. Circulation of pottery in Lecce between the 12th and 13th centuries. Islamic and Byzantine tableware glazed productions. In: Arthur P, Leo Imperiale M, editors. VII Congresso Nazionale di Archeologia Medievale, Lecce, 9–12 Settembre. Firenze: All'Insegna del Giglio. 2015. p. 251–256.
8. Vroom J. Pottery finds from a 'cess-pit' at the southern wall in Durres, central Albania. In: Böhlendorf-Arslan B, Uysal AO, Witte-Orr J, editors. Çanak. Late Antique and Medieval Pottery and Tiles in Mediterranean Archaeological Contexts. Instambul: Ege Yayınları. 2007. p. 319–334.
9. Falcone F, Cinosi A, Siverio G, Rosatelli G. New methodological XRF approach for powder microanalysis. In: International Conference on Total Reflection XRay Fluorescence Analysis and Related Methods, oral presentation, 05 08/09/2023, Clausthal Zellerfeld, Germany.
10. Palache C, Berman H, Frondel C. Dana's system of mineralogy. 7th ed. New York: John Wiley and Sons, Inc.; 1944.
11. Colomban P, Kirmizi B, Franci GS. Cobalt and associated impurities in blue (and green) glass, glaze and enamel: relationship between raw materials, processing, composition, phases and international trade. Minerals. 2021;11(6):633. https://doi.org/10.3390/min11060633.
12. Molera J, Climent-Font A, Garcia G, Pradell T, Vallcorba O, Zucchiatti A. Experimental study of historical processing of cobalt arsenide ore for colouring glazes (15th–16th century Europe). J Archaeol Sci. 2021;36:102797. https://doi.org/10.1016/j.jasrep.2021.102797.
13. Tite MS, Freestone I, Mason R, Molera J, Vendrell-Saz M, Wood N. Lead Glazes in Antiquity- Methods of production and reasons for use. Archaeometry. 1998;40(2):241–60. https://doi.org/10.1111/j.1475-4754.1998.tb00836.x.
14. Tite MS, Kilikoglou V, Vekinis G. Strenght, toughness and thermal shock resistance of ancient ceramics, and their influence on technological choice. Archaeometry. 2001;43:301–24.
15. Roedder E. Silicate liquid immiscibility in magmas. In: Yoder HS Jr, editor. Evolution of the Igneous Rocks: fiftieth anniversary perspectives. Princeton: Princeton University Press; 1979.
16. Karim MA, Ariffin A, Holland D. The role of tin in glass system. J Sci Math Technol. 2014;1(1):89–104.
17. Colomban P. Glazes and enamels. In: Richet P, editor. Encyclopedia of glass science. Technology: History and Culture Wiley; 2021. p. 524–40.
18. Pasero M, Kampf AR, Ferraris C, Pekov IV, Rakovan J, White TJ. Nomenclature of the apatite supergroup minerals. Eur J Mineral. 2010;22(2):163–79. https://doi.org/10.1127/0935-1221/2010/0022-2022.
19 Inegbenebor AJ, Thomas JH, Williams PA. The chemical stability of mimetite and distribution coefficients for pyromorphite-mimetite solid-solutions. Mineral Mag. 2018;53(371):363–371.
20. Flis J, Manecki M, Bajda T. Solubility of pyromorphite $Pb_5(PO_4)_3Cl$-mimetite $Pb_5(AsO_4)_3Cl$ solid solution series. Geochim Cosmochim Acta. 2011;75(7):1858–68. https://doi.org/10.1016/j.gca.2011.01.021.
21. Colomban P, Maggetti M, d'Albis A. Non-invasive Raman identification of crystalline and glassy phases in a 1781 Sèvres Royal Factory soft paste porcelain plate. J Eur Ceram Soc. 2018;38(15):5228–33. https://doi.org/10.1016/j.jeurceramsoc.2018.07.001.
22. Manoun B, Azdouz M, Azrour M, Essehli R, Benmokhtar S, El Ammari L, Ezzahi A, Ider A, Lazor P. Synthesis, Rietveld refinements and Raman spectroscopic studies of tricationic lacunar apatites $Na_{1-x}K_xPb_4(AsO_4)_3$ ($0 \leqslant x \leqslant 1$). J Mol Struct. 2011;986(1–3):1–9. https://doi.org/10.1016/j.molstruc.2010.09.043.
23. Matin M. Tin-based opacifiers in archaeological glass and ceramic glazes: a review and new perspectives. Archaeol Anthropol Sci. 2019;11:1155–67. https://doi.org/10.1007/s12520-018-0735-2.

24. Gradmann R, Schussler R. Composition and colouring agents of historical Islamic glazes measured with EMPA and μ-XRD. Eur J Mineral. 2015;27(3):325–35. https://doi.org/10.1127/ejm/2015/0027-2456.
25. Tite MS. Ceramic production, provenance and use- a review. Archaeometry. 2008;50(2):216–31. https://doi.org/10.1111/j.1475-4754.2008.00391.x.
26. Mason RBJ. Shine like the sun—Lustre-painted and associated pottery from the medieval Middle East. Toronto: Royal Ontario Museum; 2004.
27. Grandmann R. Analysis of Historical Islamic glazes and the development of a substitution material. Doctoral Dissertation, Institute of Geography and Geology, Department of Geodynamics and Geomaterial Research, Universitat Wurzburg. 2016.
28. Rohrs S, Dumazet A, Kuntz K, Franke U. Bodies and glazes of architectural ceramics from the Ilkhanid period at Takht-e Soleyman (North-Western Iran). Minerals. 2022;12:158. https://doi.org/10.3390/min12020158.
29. Tonghini C. Qal'at Ja'bar Pottery—A study of a Syrian fortified site of the late 11th-14th centuries. Oxford: The Council for Brithish Research in the Levant; 1998.
30. Simsek G, Unsalan O, Bayraktar K, Colomban P. On-site pXRF analysis of glaze composition and colouring agents of "Iznik" tiles at Edirne mosques (15th and 16th-centuries). Ceram Int. 2019;45(1):595–605. https://doi.org/10.1016/j.ceramint.2018.09.213.
31. Kühn H. Lead-Tin Yellow. In: Roy A, editor. Artists pigments, A handbook of their history and characteristics, vol. 2. Washington: National Gallery of Art; 1993. p. 101–10.
32. Rooksby HP. Yellow cubic lead-tin oxide opacifier in ancient glasses. J Soc Glass Technol Sect B: Phys Chem Glasses. 1964;5:20–5.
33. Gliozzo E, Ionescu C. Pigments – Lead-based whites, reds, yellows and oranges and their alteration phases. Archaeol Anthropol Sci. 2022;14:17. https://doi.org/10.1007/s12520-021-01407-z.
34 Geller RF, Creamer AS, Bunting EN. The system PbO-SiO_2. J Res Natl Bur Stand. 1934;13(2):243.
35 McMurdie HF, Hall FP. Phase diagrams for ceramists: supplement no.1. J Am Ceramic Soc. 1949. https://doi.org/10.1111/j.1151-2916.1949.tb19765.x.
36. Garner H. An early piece of glass from Eridu. Iraq. 1956;18(2):147–9.
37. Garner H. The use of imported and native cobalt in Chinese blue-and-white. Oriental Art. 1956;2(2):48–51.
38. Matin M, Pollard AM. From ore to pigment: a description of the minerals and an experimental study of cobalt ore processing from the Käshän mine Iran. Archaeometry. 2017;59(4):731–46. https://doi.org/10.1111/arcm.12272.
39 Ghorbani M. The economic geology of Iran: history of mining. Berlin: Springer, Dordrecht; 2013. https://doi.org/10.1007/978-94-007-5625-0.

Publisher's Note